



## Article

# Enhancing Light Harvesting in Dye-Sensitized Solar Cells through Mesoporous Silica Nanoparticle-Mediated Diffuse Scattering Back Reflectors

Jeffrie Fina <sup>1</sup> , Navdeep Kaur <sup>1</sup>, Chen-Yu Chang <sup>1</sup>, Cheng-Yu Lai <sup>1,2</sup> and Daniela R. Radu <sup>1,\*</sup> <sup>1</sup> Department of Mechanical and Materials Engineering, Florida International University, Miami, FL 33174, USA<sup>2</sup> Department of Chemistry and Biochemistry, Florida International University, Miami, FL 33199, USA

\* Correspondence: dradu@fiu.edu

**Abstract:** Dye-sensitized solar cells (DSSCs) hold unique promise in solar photovoltaics owing to their low-cost fabrication and high efficiency in ambient conditions. However, to improve their commercial viability, effective, and low-cost methods must be employed to enhance their light harvesting capabilities, and hence photovoltaic (PV) performance. Improving the absorption of incoming light is a critical strategy for maximizing solar cell efficiency while overcoming material limitations. Mesoporous silica nanoparticles (MSNs) were employed herein as a reflective layer on the back of transparent counter electrodes. Chemically synthesized MSNs were applied to DSSCs via bar coating as a facile fabrication step compatible with roll-to-roll manufacturing. The MSNs diffusely scatter the unused incident light transmitted through the DSSCs back into the photoactive layers, increasing the absorption of light by N719 dye molecules. This resulted in a 20% increase in power conversion efficiency (PCE), from 5.57% in a standard cell to 6.68% with the addition of MSNs. The improved performance is attributed to an increase in photon absorption which led to the generation of a higher number of charge carriers, thus increasing the current density in DSSCs. These results were corroborated with electrochemical impedance spectroscopy (EIS), which showed improved charge transport kinetics. The use of MSNs as reflectors proved to be an effective practical method for enhancing the performance of thin film solar cells. Due to silica's abundance and biocompatibility, MSNs are an attractive material for meeting the low-cost and non-toxic requirements for commercially viable integrated PVs.

**Keywords:** mesoporous silica nanoparticles; diffuse reflector; dye-sensitized solar cell; photovoltaic performance



**Citation:** Fina, J.; Kaur, N.; Chang, C.-Y.; Lai, C.-Y.; Radu, D.R. Enhancing Light Harvesting in Dye-Sensitized Solar Cells through Mesoporous Silica Nanoparticle-Mediated Diffuse Scattering Back Reflectors. *Electron. Mater.* **2023**, *4*, 124–135. <https://doi.org/10.3390/electronicmat4030010>

Academic Editor: Dong Chan Lim

Received: 4 August 2023

Revised: 23 August 2023

Accepted: 29 August 2023

Published: 30 August 2023



**Copyright:** © 2023 by the authors. Licensee MDPI, Basel, Switzerland. This article is an open access article distributed under the terms and conditions of the Creative Commons Attribution (CC BY) license (<https://creativecommons.org/licenses/by/4.0/>).

## 1. Introduction

With historically escalating global energy demands, the dependence on fossil fuels as a primary energy source has led to severe political, economic, and environmental consequences, creating an urgent need for alternative sustainable energy sources [1,2]. As the largest source of the Earth's energy budget, solar energy has been one of the leading candidates for fueling our world, prompting a photovoltaic (PV) solar cell technology boom. Dye-sensitized solar cells (DSSCs) are third-generation solar cells with key advantages such as light weight, non-toxicity, flexibility, color tuning, and processability in ambient conditions, which makes them feasible for roll-to-roll manufacturing [3,4]. Furthermore, their operability in low-light conditions makes them an attractive alternative to other PV technologies, such as silicon or perovskites, as integrated PVs for indoor and mobile device applications [5–7].

The first DSSC was reported in 1991 by Grätzel and O'Regan [8]. The standard Grätzel-type sandwich cell consists of a mesoporous TiO<sub>2</sub> (m-TiO<sub>2</sub>) photoanode sensitized by a monolayer of N719 dye molecules, an ( $I^- / I_3^-$ ) redox electrolyte, and a platinum (Pt) counter electrode (CE). The mesoporous photoanode layer, characterized by pore sizes

ranging from 2 to 50 nm in diameter, serves as the key electronic material that enables the absorption of substantial amounts of photoactive dye. This capability arises from its extensive surface area, which contributes to the impressive performance of DSSCs. While DSSCs have unique advantages, their lower absorption of incident light by sensitizer dye molecules, accompanied by recombination of photo-generated charge carriers at the photoanode–electrolyte interface, limits their power conversion efficiency (PCE). Several modifications to the structure of DSSCs have thus been researched to improve light harvesting and reduce recombination reactions, raising their PCE [9–12]. Optical modifications, like reflective layers, enhance light harvesting by reflecting unabsorbed photons back into the photoactive layers, recycling them into the system [13]. The extended path length of the photons increases the probability of absorption and charge generation, thereby raising the photocurrent and subsequently improving PCE. CE back reflectors have the key advantage of enhancing light harvesting without modifying the standard cell materials. Several types of back reflectors have thus been researched, such as metal-based mirrors and photonic crystals, showing promising results [14–18]. However, DSSC modifications must incorporate earth-abundant materials with lower fabrication costs in order to reduce their environmental impact and cost of energy.

Towards this direction, mesoporous silica nanoparticles (MSNs) have garnered increased attention as light-scattering reflective layers in DSSCs owing to their ordered porous structure, high surface area, mechanical stability, and strong light-scattering capabilities [19–21]. Light scattering layers are typically composed of dielectric nanoparticles that reflect light of a wavelength in the same order of magnitude as their particle size, as described by Mie theory [22–24]. Incorporating these nanoparticles as a photoanode overlayer was shown to successfully trap photons and improve PCE [25], but this configuration can lead to an increased thickness and concentration of grain boundaries, which in turn can raise the charge recombination rate [26]. However, despite their favorable properties for enhancing PV performance of DSSCs, MSNs have yet to be tested as external back reflectors. Employing MSNs as a CE back reflector could enhance the incident light absorption of dye sensitizers by reflecting unabsorbed light to the photoanodes, while also improving the charge transfer kinetics. Thus, a similar enhancement in light harvesting can be achieved using MSN back reflectors without altering the electronic layers of DSSCs, considering the strong light-scattering properties of MSNs along with their large surface area. The degree of scattering by MSNs determines the angular distribution of reflected light, and thus the optical performance of the reflector [27]. MSNs show increased light scattering capabilities because of reflections and refractions that occur at the interfaces between the silica pore channels and air due to their contrast in refractive index [28]. Unabsorbed photons are thereby scattered by the MSNs, extending their path length in the photoactive layers. The result is a diffuse back reflector that recycles photons and confines them within the system, improving the absorption of light [29]. Dielectric reflectors have shown superior diffuse scattering efficiency compared to metallic reflectors, with the advantage of lower cost [30]. Since DSSCs perform exceptionally well under diffuse light conditions [31], the enhanced harvesting of ambient light owing to MSN reflectors makes them suitable for low-light and indoor applications. Maintaining high efficiency in these conditions is pivotal for DSSCs to reach the photovoltage requirements needed to become an alternative energy source for portable electronics.

In this work, the PV performance of standard DSSCs was enhanced by using MSNs as a reflective scattering layer on the back of a Pt CE. Synthesized MSNs were characterized via X-ray diffraction, transmission electron microscopy, nitrogen physisorption (the Brunauer–Emmett–Teller method), dynamic light scattering, and Fourier transform infrared spectroscopy. The optical properties of MSNs were characterized by UV–visible reflectance measurements to analyze their effectiveness as a diffuse reflector. The resulting change in light harvesting when applied on DSSCs was evaluated through current density–voltage (J–V) measurements and correlated with changes in charge transport kinetics using electrochemical impedance spectroscopy (EIS).

## 2. Materials and Methods

All chemicals for this work were used as received and without further purification. For the synthesis of MSNs, hexadecyltrimethylammonium bromide (CTAB,  $\geq 99\%$ ) was purchased from Sigma-Aldrich (Saint Louis, MI, USA). Tetraethyl orthosilicate (TEOS, 99.9%) was purchased from Alfa Aesar (Haverhill, MA, USA). Sodium hydroxide (NaOH), hydrochloric acid (HCl, 37%), and methanol were purchased from ThermoFisher Scientific (Waltham, MA, USA). ACS reagent-grade nanopure water was purchased from LabChem (Zelienople, PA, USA). Ethanol (200 proof, 100% by volume) was purchased from Decon Labs (King of Prussia, PA, USA). For DSSC fabrication, fluorine-doped tin oxide (FTO) substrates were purchased from Hartford Glass Co., Inc., titanium (IV) isopropoxide (TTIP) and titanium dioxide ( $\text{TiO}_2$ ) paste from Sigma-Aldrich (Saint Louis, MI, USA), Platisol-T from Solaronix (Aubonne, Switzerland), Di-tetrabutylammonium cis-bis(isothiocyanato)bis(2,2'-bipyridyl-4,4'-dicarboxylato) ruthenium(II) (N719) dye, and EL-HSE electrolyte from Greatcell Solar Co. Ltd. (Queanbeyan, Australia). Butvar B-98 (PVB) binder was purchased from TALAS (Brooklyn, NY, USA).

The MSNs synthesized in this work were characterized by a variety of analytical methods to understand how these features contribute to their light scattering capabilities. Evaluation of MSNs by X-ray diffraction (XRD) is customary for this class of materials given their parallel pores, packed in hexagonal arrays, that confer the material a significant structural order leading to diffraction under X-ray. The XRD measurements were conducted on a Rigaku MiniFlex 600 equipped with Cu  $K_\alpha$  radiation ( $\lambda = 1.5405 \text{ \AA}$ ) operating at 40 mV and 30 mA. MSN particle size and morphology were analyzed using a JEOL/JEM-2100 (200 kV) transmission electron microscope (TEM). The specific surface area, pore volume, and pore size distribution of MSNs were determined via the Brunauer–Emmett–Teller (BET) and density functional theory (DFT) methods using nitrogen adsorption–desorption isothermal curves on a Quantachrome/NOVAtouch LX-2. Average particle size measurements of MSNs were performed using dynamic light scattering (DLS) with a Malvern Zetasizer Nano-ZS ZEN3600 operated at room temperature. Fourier transform infrared spectroscopy with attenuated total reflection (FTIR-ATR) was performed to characterize the chemical bonds in MSNs and verify the removal of CTAB surfactant template from the pores after the acid washing step. Cross-sectional imaging of the DSSC layers and MSN film microstructure was performed with a JEOL/JSM-F100 Schottky field emission scanning electron microscope (FE-SEM). Optical spectroscopy of the MSNs' diffuse reflectance properties, absorbance of CEs, and transmittance of the DSSC layers was performed using a Shimadzu UV-3600 Plus spectrophotometer using an integrating sphere, where full DSSCs with a large effective area of  $3 \text{ cm}^2$  were fabricated to fit the aperture of the spectrophotometer.

The PV performance of the fabricated DSSCs was evaluated under 1 sun conditions (1.5 G AM) at an intensity of  $100 \text{ mW/cm}^2$  using an ORIEL LCS-100TM solar simulator calibrated with a standard silicon cell and connected to a Keithley source meter (Model 2400), providing J-V curves from which the  $V_{OC}$ ,  $J_{SC}$ , FF, and PCE can be measured under operation. Electrochemical impedance spectroscopy (EIS) potentiostatic measurements were performed under illumination in a frequency range of 0.1 Hz to 1 MHz using a  $\Omega$  Metrohm Autolab to obtain the interfacial impedance and electron lifetime in the DSSC layers, allowing for the analysis of the charge transfer kinetics.

**Synthesis of MSNs.** MSNs were synthesized following a modified procedure from the literature [32–34]. This procedure was chosen due to the long-range order of hexagonal pores that extend in parallel along the synthesized spheroidal particles. In a typical experiment, 2.00 g (5.48 mmol) of CTAB was added to a solution containing 0.56 g (14.0 mmol) NaOH dissolved in 480 mL of nanopure water. The solution was heated to  $85 \text{ }^\circ\text{C}$  and stirred for 1 h to completely dissolve the CTAB. Then, 10 mL of TEOS was rapidly injected into the solution and stirred at  $85 \text{ }^\circ\text{C}$  for 2 h, precipitating into a white suspension of MSN–CTAB. The precipitate was filtered and rinsed twice with nanopure water and once with methanol, then dried overnight in a vacuum oven. Subsequently, 1.5 g of the MSN–CTAB was refluxed in a solution containing 160 mL of methanol and 9 mL of HCl (37%) (18:1 v/v) for 24 h at

75 °C to remove the surfactant template (CTAB). The resulting MSN hot suspension was then filtered, rinsed three times with methanol, and left to dry overnight.

**Photoanode Preparation.** FTO substrates were patterned via chemical etching, where zinc paste (100 mg Zn powder + 0.5 mL nanopure H<sub>2</sub>O) was deposited on the FTO layer and etched with aqueous HCl (18.5% *v/v*) added dropwise, then rinsed with nanopure water. To ensure the removal of surface contaminants, the patterned substrates were thoroughly cleaned by ultrasonication in the following steps: (1) a soap solution of Hellmanex III in nanopure water (2%), (2) nanopure water, (3) acetone, (4) ethanol, and (5) isopropanol at 80 °C; at each step, the substrates were cleaned for 15 min and dried under nitrogen flow. The substrates were treated with an MTI EQ-PCE-66 UV ozone cleaner for 30 min to further remove organic surface contaminants and ensure proper adhesion of the TiO<sub>2</sub> layer with FTO. A compact layer of TiO<sub>2</sub> (c-TiO<sub>2</sub>) was deposited via the spray pyrolysis method, where 0.4 M solution of TTIP was sprayed on the effective area of pre-annealed substrates at 450 °C, and then further annealed at 450 °C for 30 min to remove the organic compounds in the precursor and crystallize into the c-TiO<sub>2</sub> layer. This serves as an interfacial layer between the m-TiO<sub>2</sub> and FTO, as interfaces between the FTO–m-TiO<sub>2</sub> and FTO–electrolyte act as recombination sites for photo-generated charge carriers. TiO<sub>2</sub> paste was applied on top of the c-TiO<sub>2</sub> layer via doctor blading and annealed at 450 °C for 60 min to remove the surfactant template and crystallize into a mesoporous TiO<sub>2</sub> layer (m-TiO<sub>2</sub>), using a mask to produce an effective area of 0.15 cm<sup>2</sup>. The thickness of c-TiO<sub>2</sub> and m-TiO<sub>2</sub> films were measured with cross-sectional FE-SEM imaging to be 60 nm and 11.6 μm, respectively (see Figure 1). The m-TiO<sub>2</sub> layers were sensitized by submerging the substrates in photoactive N719 dye (0.4 mM) for 20 h and then rinsing with ethanol to remove excess dye from the pores.

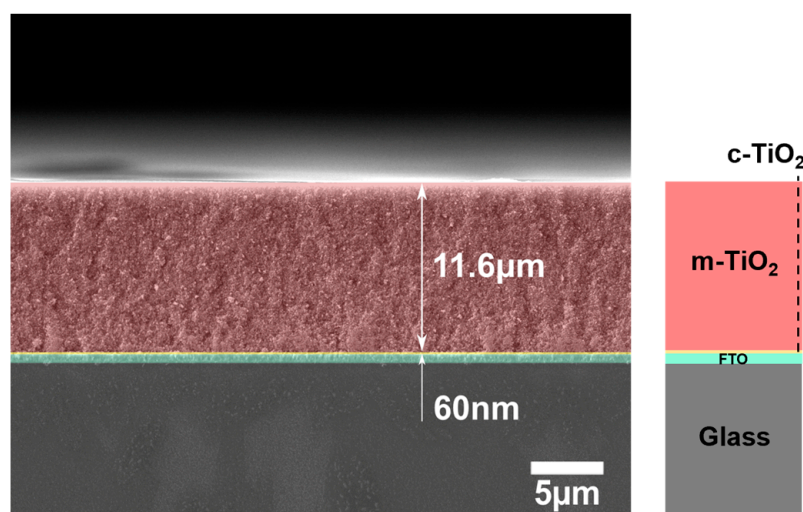


**Figure 1.** Cross-sectional SEM image of c-TiO<sub>2</sub> and m-TiO<sub>2</sub> films.

**Counter Electrode Preparation.** FTO substrates were cleaned with the same procedure as the photoanodes. An amount of 30 μL of Plastisol-T was drop-casted onto the substrate and annealed at 450 °C for 30 min to obtain a Pt catalytic layer. This layer catalyzes the reduction of electrolyte at the counter electrode while ensuring rapid and efficient charge transport, which is essential for the overall performance of the device. The MSN reflector solution was prepared by dissolving 25 mg of PVB in 1.5 mL of ethanol and then adding 350 mg of MSNs. PVB was chosen as a binder for the MSNs thanks to its high performance in optical coatings and adhesion with silica. Ethanol acts as an effective solvent for both PVB and MSNs while also providing an adequate evaporation rate at room temperature, allowing for the facile fabrication of smooth and uniform reflector films. The solution was stirred for 1 h until homogeneous and then applied onto the glass side of the Pt coated CE substrate via bar coating. The thickness of the Pt and MSNs films were 25 nm and 50 μm, respectively, as measured by FE-SEM and shown in Figure 2. The photoanode and CE are

clipped together with the sensitized m-TiO<sub>2</sub> layer facing the Pt layer, minimizing the gap between these layers to reduce the diffusion distance for electrolyte species. The I<sup>-</sup>/I<sub>3</sub><sup>-</sup> redox electrolyte was then inserted via pipette into the gap between the two electrodes, where it infiltrates the mesoporous TiO<sub>2</sub> structure to serve as a mediator between the N719 dye molecules and Pt CE. The DSSCs were assembled in a sandwich architecture, shown in Figure 3, where light is initially absorbed by the photoanode, and then unabsorbed light is reflected by the MSN film.

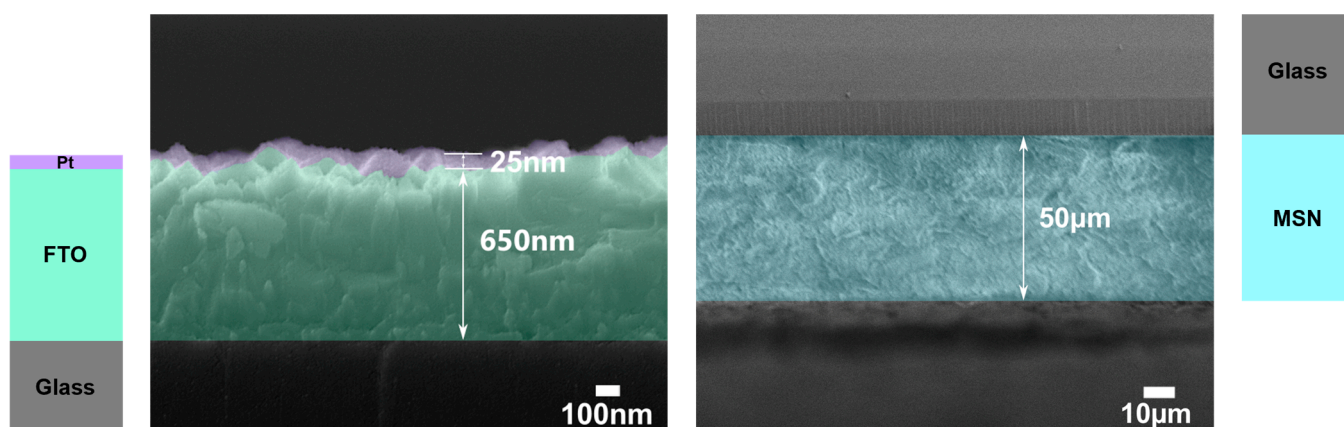


Figure 2. Cross-sectional SEM image of Pt and MSN films.

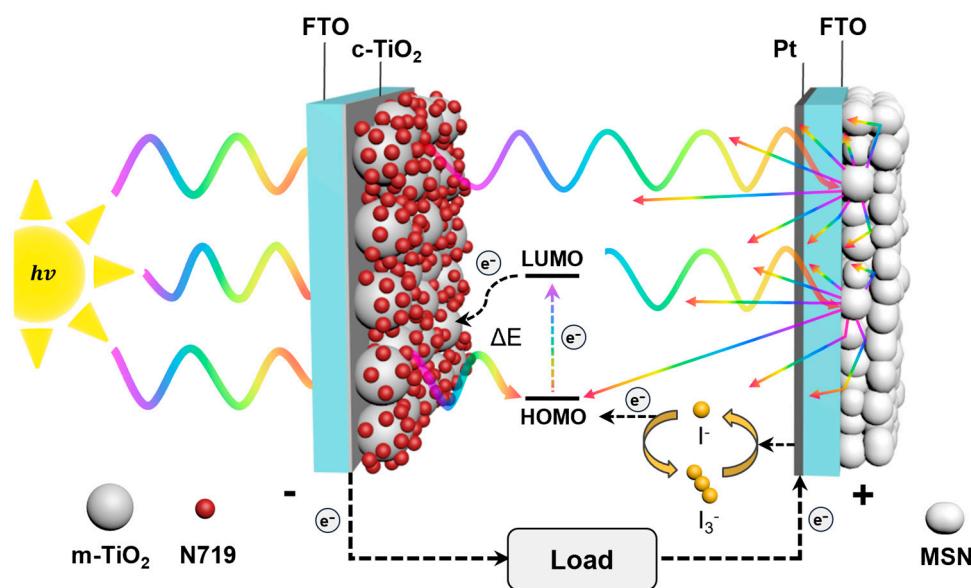
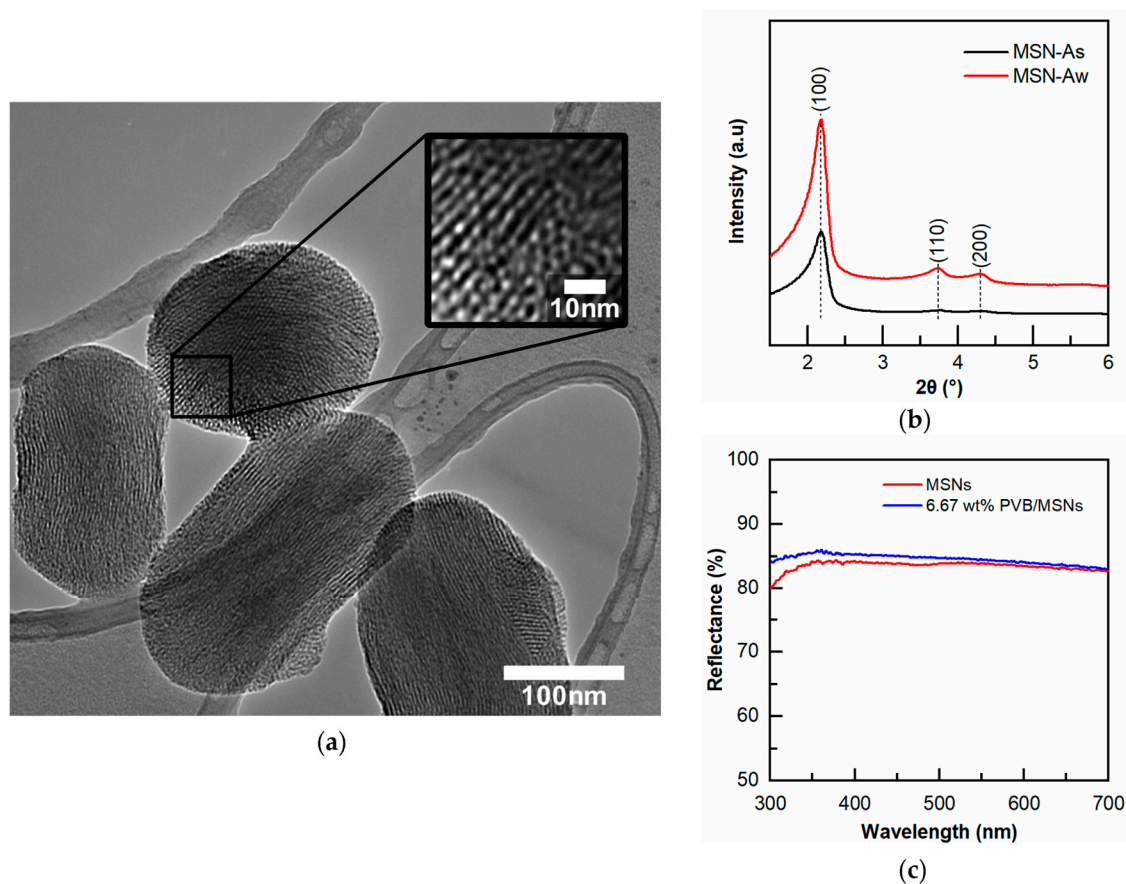


Figure 3. Concept visualization of DSSCs with MSN reflector films.

### 3. Results

#### 3.1. MSNs Characterization

Figure 4a shows TEM images of MSNs with an elongated spheroid morphology and an average particle size of ~300 nm. Pore channels were observed with long range order and in parallel along the semimajor axis. N<sub>2</sub> adsorption/desorption measurements (Figure S1) showed a typical type IV isotherm with no hysteresis, indicative of a mesoporous network of narrow width. The specific surface area calculated by the BET method was 1119 m<sup>2</sup>·g, while the pore size distribution calculated by the DFT method indicated a uniform average pore diameter of 4.1 nm. DLS measurements (Figure S2) showed a particle size of 281 nm with a standard deviation of ±53 nm.



**Figure 4.** (a) TEM image of MSNs with inset showing the parallel pores. (b) XRD spectrum of MSNs as synthesized (MSN-As) and after acid wash (MSN-Aw). (c) UV-visible reflectance spectrum of MSNs.

The low-angle XRD diffraction pattern is shown in Figure 4b and has the characteristic MSN peak at  $2\theta = 2.18^\circ$  Bragg's angle corresponding to the (100) diffraction lattice plane of ordered hexagonal porous structures [35]. Two additional peaks are observed at  $2\theta = 3.73^\circ$  and  $2\theta = 4.30^\circ$ , which are attributed to the (110) and (200) lattice planes, respectively, indicative of the long-range order of the pore structure. FTIR spectroscopy (Figure S3) of MSNs, MSN-CTAB, and MSN-PVB powder showed silicon dioxide absorption peaks at  $1050\text{ cm}^{-1}$  and  $798\text{ cm}^{-1}$  corresponding to the vibration of Si-O-Si and Si-O bonds, respectively [36,37]. The absence of the CTAB C-N vibration peak at  $1479\text{ cm}^{-1}$  in the MSN spectrum confirmed the removal of surfactant from the mesopores after the acid washing step (as shown in the supporting information).

To investigate the light scattering properties of MSNs, a diffuse reflectance measurement was performed via UV-visible spectroscopy, shown in Figure 4c. The spectrum showed  $>80\%$  reflectance in the visible range, coinciding with the absorbance range of the N719 dye (350–700 nm) [38]. MSNs with 6.67 wt% PVB were also characterized to determine the effect of binder on light scattering and showed the same magnitude of reflectance with a slight increase in the visible and UV range.

FE-SEM imaging of the MSN reflector microstructure (Figure 5a) shows the arrangement of randomly oriented particles that compose the film. To determine the amount of light being trapped by MSN reflectors applied to DSSCs, UV-visible transmittance measurements were performed (Figure 5b), which demonstrated a highly reduced transmittance in the N719 dye photoactive range compared to a reference DSSC.

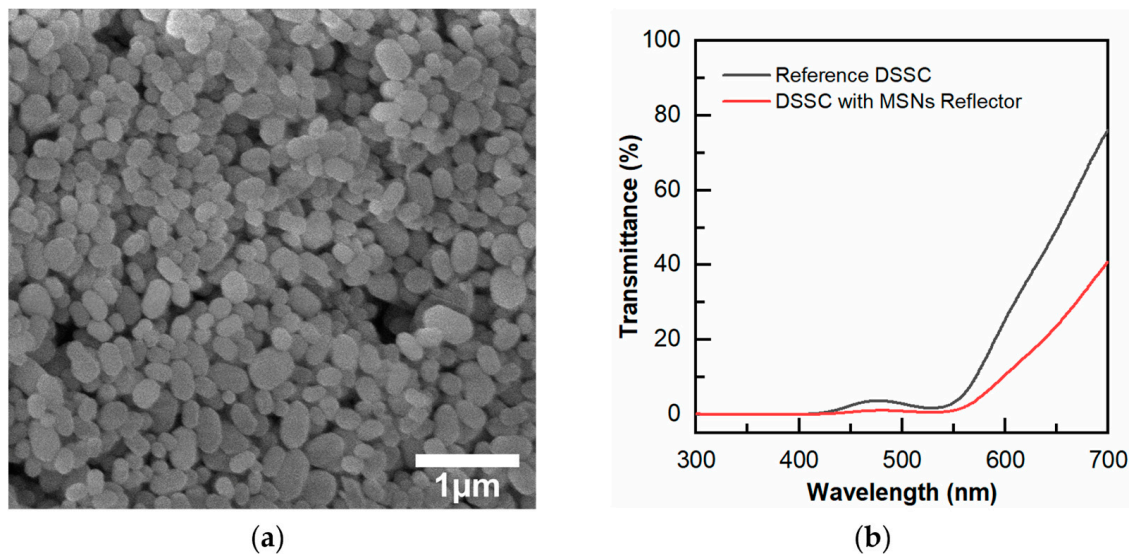


**Figure 5.** (a) FE-SEM image of MSN reflector microstructure (b) UV–visible transmittance spectrum of full DSSCs with and without MSN reflectors.

### 3.2. Photovoltaic Measurements

The derived PV parameters, including current density ( $J_{SC}$ ), open-circuit voltage ( $V_{OC}$ ), fill factor (FF), and PCE, are summarized in Table 1. With the addition of MSNs as reflectors, the PCE of DSSCs was improved to 6.68% from a reference PCE of 5.57%, showing a 20% increase. This is correlated with an increase in  $J_{SC}$  from 12.41 mA/cm<sup>2</sup> in reference to 14.60 mA/cm<sup>2</sup> with an MSN reflector. These results indicate that the scattering properties of MSNs were successfully employed to diffusely reflect unabsorbed light, extending their path length in the photoactive layers, and thereby increasing the absorption and photocurrent. The  $V_{OC}$  also showed a marginal increase from 0.66 V in reference to 0.68 V with MSN reflectors, while the FF remained consistent. The current density versus voltage (J-V) characteristics are plotted in Figure 6a.

**Table 1.** PV Parameters of DSSCs with and without MSN reflectors.

Device Configuration	$J_{SC}$ (mA/cm <sup>2</sup> )	$V_{OC}$ (V)	FF	PCE (%)
FTO/c-TiO <sub>2</sub> /m-TiO <sub>2</sub> /N719/Electrolyte/Pt/FTO	12.41	0.66	0.67	5.57
FTO/c-TiO <sub>2</sub> /m-TiO <sub>2</sub> /N719/Electrolyte/Pt/FTO/MSNs	14.60	0.68	0.67	6.68

To verify the reproducibility of DSSCs enhanced by MSN reflectors, ten reference devices and ten devices with MSN reflectors were fabricated. Shown in Figure 6b, the MSN reflectors reliably increased the PCE, with a deviation of  $\pm 0.2\%$ . For all enhanced devices, the  $J_{SC}$  was increased with a deviation of  $\pm 0.7$  mA/cm<sup>2</sup>. The narrow deviation in these results indicate that this method is a reliable option for boosting DSSC performance.

### 3.3. Charge Transport Measurements

The PV performance was further evaluated by analyzing the charge transfer mechanisms using EIS measurements, with the charge transfer resistances and electron lifetime summarized in Table 2. Nyquist and Bode plots were obtained under illumination using the obtained  $V_{OC}$  values to estimate the charge transport kinetics within the cell. The Nyquist plots, shown in Figure 6c, show two semicircles fitted with an equivalent circuit model (Inset of Figure 6c), where Q is the constant phase element. The diameter of the first semicircle in the high-frequency range is the charge transfer resistance at the CE–electrolyte interface ( $R_1$ ) and the diameter of the second semicircle in the low-frequency range is the resistance at the photoanode–electrolyte interface ( $R_2$ ). The series resistance ( $R_s$ ) is obtained

from the real-axis intercept of the high-frequency semicircle. A decrease in  $R_2$  is observed with the addition of MSN reflectors, indicating reduced resistance for the transport of electrons in the photoanode, which is in congruence with the increased  $J_{SC}$ . A marginal increase in  $R_1$  is also observed, likely as a result of increasing temperature due to absorption of reflected photons by the CE layers, as measured by UV-vis absorbance of the CEs with and without MSN reflectors (Figure S4).

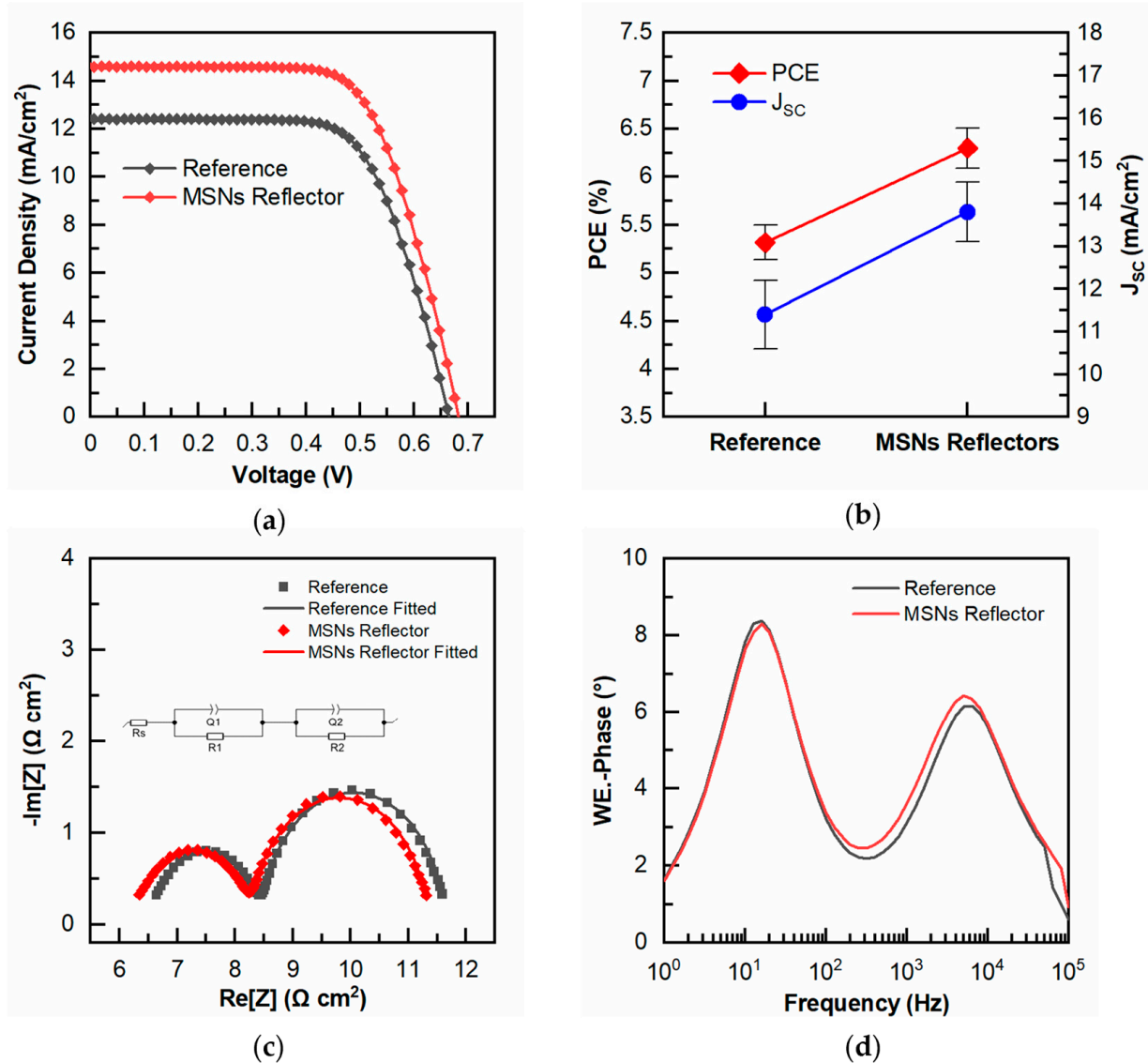


**Figure 6.** (a) J-V curves of reference DSSCs and DSSCs with MSN reflector films. (b) Reproducibility of reference DSSCs and DSSCs with MSN reflector films. (c) Nyquist plots of reference DSSCs and DSSCs with MSN reflectors fitted with the equivalent circuit model. (d) Bode plots of reference DSSCs and DSSCs with MSN reflector films.

**Table 2.** PV Parameters of DSSCs with and without MSN reflectors.

Device Configuration	$R_1$ (Ω · cm <sup>2</sup> )	$R_2$ (Ω · cm <sup>2</sup> )	$R_s$ (Ω · cm <sup>2</sup> )	$\tau$ (ms)
FTO/c-TiO <sub>2</sub> /m-TiO <sub>2</sub> /N719/Electrolyte/Pt/FTO	1.81	3.17	6.62	10.1
FTO/c-TiO <sub>2</sub> /m-TiO <sub>2</sub> /N719/Electrolyte/Pt/FTO/MSNs	1.93	3.09	6.30	10.1

To further elucidate the charge transport kinetics, the electron lifetime in the photoanode-electrolyte interface was estimated from the maximum angular frequency ( $\omega_{max}$ ) using Equation (1):

$$\tau = \frac{1}{\omega_{max}} = \frac{1}{2\pi f_{max}} \quad (1)$$

where  $f_{max}$  is the maximum frequency in the low frequency region of the Bode plot (Figure 6d). The electron lifetime remained the same after the addition of MSN reflectors, suggesting that the rate of recombination was not significantly affected.

#### 4. Discussion

MSNs have unique optical properties due to their size, morphology, and mesoporous structure. The particle size of ~300 nm measured by TEM and DLS is reported to produce Mie scattering of light in the visible range [22,39–41]. Moreover, the spheroidal morphology and geometrical irregularities on the particle surface amplify backward scattering [42–44]. The large specific surface area as calculated by the BET method exceeds 1100 m<sup>2</sup>/g, while the pore size distribution calculated by the DFT method indicates a uniform average of pores. As showed by the TEM images, the MSNs showcase uniform parallel pores which contributes to the light management, as could be inferred from the ability of these overall amorphous materials to exhibit X-ray diffraction. The sum of these properties increases the diffuse reflectance of MSNs, which showed that ~85% of light in the visible range is reflected. These results indicate that the optical properties of MSNs are closely aligned with the requirements for reflective layers in DSSCs. When applied as a reflector film, the multi-oriented mesoporous particles act as multiple scattering modes that confine unabsorbed light within the system [45]. The UV–visible transmittance of a DSSC with MSN reflector showed a significant portion of light being trapped, with near-zero transmittance from 300–550 nm. This confirms that MSNs recycle unabsorbed light back into the photoactive layers, serving as an effective light trapping layer for increasing light absorption.

The addition of MSN reflectors reliably enhanced light harvesting in DSSCs, as evidenced by the increased PCE and  $J_{SC}$ . Photons are diffusely reflected by the MSN, extending their path length and rate of absorption in the sensitized film, thereby increasing the concentration of charge carriers according to published reports in the field [46,47]. As a result, the introduction of MSNs led to an increase in the photocurrent of the device, driven by its significant dependence on the quantity of absorbed photons, in direct correlation with the photocurrent. The decrease in  $R_2$  indicates an improvement in the electron transport rate owing to reduced impedance at the photoanode–electrolyte interface [48,49]. Since there was no change in the electron lifetime at this interface, the reduced impedance can be attributed to a decrease in the diffusion resistance across the m-TiO<sub>2</sub> layer, corroborating the improved charge transport kinetics and facilitating the generation of a higher photocurrent [50,51]. The increased  $V_{OC}$  is likely caused by an increase in temperature due to the absorption of photons by the CE layers. This is supported by the increase in  $R_1$ , which corresponds to the counter electrode–electrolyte interface, along with UV–visible absorbance measurements of CEs that showed increased absorbance of visible light with the addition of MSNs.

These results agree with the existing literature for DSSC back reflectors. Zdyb and Krawczak, for instance, achieved a 15.7% increase in PCE with a 19.7% increase in  $J_{SC}$  by using BaSO<sub>4</sub> as a back reflector on DSSCs using N719 dye, and obtained even larger increases in PCE when used on alternative sensitizing dyes [52]. This speaks to the promise that highly reflective materials have for increasing light harvesting in solar cells. Employing materials with low-cost and simple fabrication, such as MSNs, is crucial for the integration of this method into existing and future PV technologies. Such methods that achieve high PCE in DSSCs are an essential requirement for their use in portable electronics, as the output of energy must be sufficient to balance the costs of fabrication and implementation.

#### 5. Conclusions

In conclusion, MSNs were successfully employed as scattering back reflectors in DSSCs, resulting in their improved light harvesting capability by reusing unabsorbed incident light and hence enhancing the overall PCE of DSSCs. The synthesized MSNs exhibited significant

diffuse reflectance of visible light, coinciding with the absorption range of N719 dye. The uniform, parallel pores of MSNs coated in thin films facilitated the trapping of unabsorbed photons and reflected them back into the photoactive layers, increasing light absorption. As a result, MSN reflectors successfully improved the performance of DSSCs, showing a 20% increase in PCE from a reference 5.57% to 6.68%. The main contributor to this enhancement is the  $J_{SC}$ , which increased from 12.41 mA/cm<sup>2</sup> in the reference cell to 14.60 mA/cm<sup>2</sup> with MSNs, owing to their diffuse reflectance of unabsorbed photons. Other performance parameters, such as  $V_{OC}$  and charge transport rate, were also improved, demonstrating additional benefits from the implementation of MSN reflectors, as the enhanced flow of electrons through the device layers improved the overall operation of the device.

The use of MSNs as a CE back reflector was demonstrated to be an effective method for boosting the performance of thin film solar cells. This heightens the viability of DSSCs for integration into electronic devices, as the increased harvesting of ambient light enhances their performance in indoor and low-light conditions. Improving the efficiency of PV energy conversion is essential for the commercial viability and widespread adoption of emergent PV technology. Additional research into the optimization of nanoparticle properties, materials, and fabrication methods could further enhance the performance of diffuse back reflectors. Investigations into the scalability of MSN reflectors and their compatibility with industrial manufacturing methods are still necessary to gain further understanding of the role these reflectors play in developing solar cell technology.

**Supplementary Materials:** The following supporting information can be downloaded at: <https://www.mdpi.com/article/10.3390/electronicmat4030010/s1>, Figure S1. MSN Nitrogen porosity measurements; Figure S2. DLS distribution curve of MSNs dispersed in ethanol; Figure S3. FTIR spectra of MSN before and after surfactant removal; and after formulated into PVB; Figure S4. UV–visible absorbance spectrum of platinum counter electrodes with and without MSN reflector film.

**Author Contributions:** Conceptualization: J.F., N.K., C.-Y.L. and D.R.R.; methodology: J.F. and N.K.; formal analysis, J.F., N.K. and C.-Y.C.; data curation, J.F., N.K. and C.-Y.C.; writing—original draft preparation, J.F. and N.K.; writing—review and editing, D.R.R. and C.-Y.L.; supervision, D.R.R. and C.-Y.L.; project administration, D.R.R.; funding acquisition, D.R.R. and C.-Y.L. All authors have read and agreed to the published version of the manuscript.

**Funding:** This material is based upon work supported in part by NASA Award #80NSSC19M0201, NASA Award #80NSSC21M0310, and the National Science Foundation under Grant No. DMR-2122078 and Grant No. CBET-1924412.

**Data Availability Statement:** Data is available from the authors upon reasonable request.

**Acknowledgments:** The authors thank Jake Carrier for help in collecting and analyzing the BET and DFT data.

**Conflicts of Interest:** The authors declare no conflict of interest. The funders had no role in the design of the study; in the collection, analyses, or interpretation of data; in the writing of the manuscript; or in the decision to publish the results.

## References

1. Intergovernmental Panel on Climate Change; Working Group I; Masson-Delmotte, V.R. *Climate Change 2021: The Physical Science Basis: The Working Group I Contribution to the Sixth Assessment Report of the Intergovernmental Panel on Climate Change*; IPCC (Intergovernmental Panel on Climate Change): Geneva, Switzerland, 2021.
2. Intergovernmental Panel on Climate Change; Working Group III. *Climate Change 2022: Mitigation of Climate Change: The Working Group III Contribution to the Sixth Assessment Report of the Intergovernmental Panel on Climate Change*; IPCC (Intergovernmental Panel on Climate Change): Geneva, Switzerland, 2022.
3. Weerasinghe, H.C.; Huang, F.Z.; Cheng, Y.B. Fabrication of flexible dye sensitized solar cells on plastic substrates. *Nano Energy* **2013**, *2*, 174–189. [[CrossRef](#)]
4. Parisi, M.L.; Maranghi, S.; Basosi, R. The evolution of the dye sensitized solar cells from Gratzel prototype to up-scaled solar applications: A life cycle assessment approach. *Renew. Sustain. Energy Rev.* **2014**, *39*, 124–138. [[CrossRef](#)]
5. Munoz-Garcia, A.B.; Benesperi, I.; Boschloo, G.; Concepcion, J.J.; Delcamp, J.H.; Gibson, E.A.; Meyer, G.J.; Pavone, M.; Pettersson, H.; Hagfeldt, A.; et al. Dye-sensitized solar cells strike back. *Chem. Soc. Rev.* **2021**, *50*, 12450–12550. [[CrossRef](#)] [[PubMed](#)]

6. Haridas, R.; Velore, J.; Pradhan, S.C.; Vindhyasarumi, A.; Yoosaf, K.; Soman, S.; Unni, K.N.N.; Ajayaghosh, A. Indoor light-harvesting dye-sensitized solar cells surpassing 30% efficiency without co-sensitizers. *Mater. Adv.* **2021**, *2*, 7773–7787. [[CrossRef](#)]
7. Li, G.; Sheng, L.; Li, T.Y.; Hu, J.; Li, P.W.; Wang, K.Y. Engineering flexible dye-sensitized solar cells for portable electronics. *Sol. Energy* **2019**, *177*, 80–98. [[CrossRef](#)]
8. Oregan, B.; Gratzel, M. A Low-Cost, High-Efficiency Solar-Cell Based on Dye-Sensitized Colloidal TiO<sub>2</sub> Films. *Nature* **1991**, *353*, 737–740. [[CrossRef](#)]
9. Gong, J.W.; Sumathy, K.; Qiao, Q.Q.; Zhou, Z.P. Review on dye-sensitized solar cells (DSSCs): Advanced techniques and research trends. *Renew. Sustain. Energy Rev.* **2017**, *68*, 234–246. [[CrossRef](#)]
10. Ramasamy, P.; Kim, J. Combined plasmonic and upconversion rear reflectors for efficient dye-sensitized solar cells. *Chem. Commun.* **2014**, *50*, 879–881. [[CrossRef](#)]
11. Li, W.; Tan, X.Y.; Zhu, J.L.; Xiang, P.; Xiao, T.; Tian, L.H.; Yang, A.B.; Wang, M.; Chen, X.B. Broadband antireflective and superhydrophobic coatings for solar cells. *Mater. Today Energy* **2019**, *12*, 348–355. [[CrossRef](#)]
12. Fathima, M.I.; Wilson, K.S.J. Efficiency Enhancement in Dye Sensitized Solar Cell Using 1D Photonic Crystal. *Silicon* **2022**, *14*, 4283–4289. [[CrossRef](#)]
13. Lee, Y.L.; Chen, C.L.; Chong, L.W.; Chen, C.H.; Liu, Y.F.; Chi, C.F. A platinum counter electrode with high electrochemical activity and high transparency for dye-sensitized solar cells. *Electrochem. Commun.* **2010**, *12*, 1662–1665. [[CrossRef](#)]
14. Lee, B.; Hwang, D.K.; Guo, P.J.; Ho, S.T.; Buchholtz, D.B.; Wang, C.Y.; Chang, R.P.H. Materials, Interfaces, and Photon Confinement in Dye-Sensitized Solar Cells. *J. Phys. Chem. B* **2010**, *114*, 14582–14591. [[CrossRef](#)] [[PubMed](#)]
15. Liu, W.; Ma, H.L.; Walsh, A. Advance in photonic crystal solar cells. *Renew. Sustain. Energy Rev.* **2019**, *116*, 109436. [[CrossRef](#)]
16. Ibrahim, I.; Lim, H.N.; Wan, N.W.K.; Huang, N.M.; Lim, S.P.; Busayaporn, W.; Nakajima, H. Plasmonic silver sandwich structured photoanode and reflective counter electrode enhancing power conversion efficiency of dye-sensitized solar cell. *Sol. Energy* **2021**, *215*, 403–409. [[CrossRef](#)]
17. Kaur, N.; Syed, F.M.; Fina, J.; Lai, C.Y.; Radu, D.R. Ag Reflectors: An Effective Approach to Improve Light Harvesting in Dye Sensitized Solar Cells. *IEEE J. Photovolt.* **2023**, *13*, 250–253. [[CrossRef](#)]
18. Kaur, N.; Oyon, S.A.; Lai, C.Y.; Radu, D.R. From reflection to absorption: Improving light harvesting of dye sensitized solar cells with Cu nanowires as reflectors. *Opt. Mater.* **2023**, *142*, 114074. [[CrossRef](#)]
19. Chen, H.W.; Chiang, Y.D.; Kung, C.W.; Sakai, N.; Ikegami, M.; Yamauchi, Y.; Wu, K.C.W.; Miyasaka, T.; Ho, K.C. Highly efficient plastic-based quasi-solid-state dye-sensitized solar cells with light-harvesting mesoporous silica nanoparticles gel-electrolyte. *J. Power Sources* **2014**, *245*, 411–417. [[CrossRef](#)]
20. Tanvi; Mahajan, A.; Bedi, R.K.; Kumar, S.; Saxena, V.; Aswal, D.K. Efficiency enhancement in dye sensitized solar cells using dual function mesoporous silica as scatterer and back recombination inhibitor. *Chem. Phys. Lett.* **2016**, *658*, 276–281. [[CrossRef](#)]
21. Ryu, J.; Yun, J.; Lee, J.; Lee, K.; Jang, J. Hierarchical mesoporous silica nanoparticles as superb light scattering materials. *Chem. Commun.* **2016**, *52*, 2165–2168. [[CrossRef](#)]
22. Zhang, Q.F.; Myers, D.; Lan, J.L.; Jenekhe, S.A.; Cao, G.Z. Applications of light scattering in dye-sensitized solar cells. *Phys. Chem. Chem. Phys.* **2012**, *14*, 14982–14998. [[CrossRef](#)]
23. Yu, I.G.; Kim, Y.J.; Kim, H.J.; Lee, C.; Lee, W.I. Size-dependent light-scattering effects of nanoporous TiO<sub>2</sub> spheres in dye-sensitized solar cells. *J. Mater. Chem.* **2011**, *21*, 532–538. [[CrossRef](#)]
24. Wang, M.; Ye, X.Y.; Wan, X.; Liu, Y.T.; Xie, X.M. Brilliant white polystyrene microsphere film as a diffuse back reflector for solar cells. *Mater. Lett.* **2015**, *148*, 122–125. [[CrossRef](#)]
25. Ito, S.; Murakami, T.N.; Comte, P.; Liska, P.; Gratzel, C.; Nazeeruddin, M.K.; Gratzel, M. Fabrication of thin film dye sensitized solar cells with solar to electric power conversion efficiency over 10%. *Thin Solid Film.* **2008**, *516*, 4613–4619. [[CrossRef](#)]
26. Zhang, Q.F.; Cao, G.Z. Hierarchically structured photoelectrodes for dye-sensitized solar cells. *J. Mater. Chem.* **2011**, *21*, 6769–6774. [[CrossRef](#)]
27. Barugkin, C.; Beck, F.J.; Catchpole, K.R. Diffuse reflectors for improving light management in solar cells: A review and outlook. *J. Opt.* **2017**, *19*, 014001. [[CrossRef](#)]
28. Fu, J.K.; Wang, Y.; Zhu, Y.C. Broadband and high diffuse reflectivity of hollow mesoporous silica nanospheres and their UV light shielding ability for light-labile peroxides. *Mater. Lett.* **2015**, *153*, 89–91. [[CrossRef](#)]
29. Usami, A. Theoretical simulations of optical confinement in dye-sensitized nanocrystalline solar cells. *Sol. Energy Mater. Sol. Cells* **2000**, *64*, 73–83. [[CrossRef](#)]
30. Fu, S.M.; Lai, Y.C.; Tseng, C.W.; Yan, S.L.; Zhong, Y.K.; Shen, C.H.; Shieh, J.M.; Li, Y.R.; Cheng, H.C.; Chi, G.C.; et al. Approaching conversion limit with all-dielectric solar cell reflectors. *Opt. Express* **2015**, *23*, A106–A117. [[CrossRef](#)]
31. Freitag, M.; Teuscher, J.; Saygili, Y.; Zhang, X.; Giordano, F.; Liska, P.; Hua, J.; Zakeeruddin, S.M.; Moser, J.E.; Gratzel, M.; et al. Dye-sensitized solar cells for efficient power generation under ambient lighting. *Nat. Photonics* **2017**, *11*, 372–378. [[CrossRef](#)]
32. Lai, C.Y.; Trewyn, B.G.; Jeftinija, D.M.; Jeftinija, K.; Xu, S.; Jeftinija, S.; Lin, V.S.Y. A mesoporous silica nanosphere-based carrier system with chemically removable CdS nanoparticle caps for stimuli-responsive controlled release of neurotransmitters and drug molecules. *J. Am. Chem. Soc.* **2003**, *125*, 4451–4459. [[CrossRef](#)]
33. Na, H.; Venedicto, M.; Chang, C.Y.; Carrier, J.; Lai, C.Y. Infrared-Activated Bactericide: Rhenium Disulfide (ReS<sub>2</sub>)-Functionalized Mesoporous Silica Nanoparticles. *ACS Appl. Bio Mater.* **2023**, *6*, 1577–1585. [[CrossRef](#)] [[PubMed](#)]

34. Venedicto, M.; Carrier, J.; Na, H.; Chang, C.Y.; Radu, D.R.; Lai, C.Y. Disulfide-Modified Mesoporous Silica Nanoparticles for Biomedical Applications. *Crystals* **2023**, *13*, 1067. [[CrossRef](#)]
35. Lu, C.; Yang, H.M.; Wang, J.; Tan, Q.; Fu, L.J. Utilization of iron tailings to prepare high -surface area mesoporous silica materials. *Sci. Total Environ.* **2020**, *736*, 139483. [[CrossRef](#)] [[PubMed](#)]
36. Nairi, V.; Medda, S.; Piludu, M.; Casula, M.F.; Vallet-Regi, M.; Monduzzi, M.; Salis, A. Interactions between bovine serum albumin and mesoporous silica nanoparticles functionalized with biopolymers. *Chem. Eng. J.* **2018**, *340*, 42–50. [[CrossRef](#)]
37. Olabisi, O.; Adewale, K. *Handbook of Thermoplastics*, 2nd ed.; CRC Press, Taylor & Francis Group: Boca Raton, FL, USA, 2016; Volume xvii, 994p.
38. Wen, P.H.; Han, Y.F.; Zhao, W.X. Influence of TiO<sub>2</sub> Nanocrystals Fabricating Dye-Sensitized Solar Cell on the Absorption Spectra of N719 Sensitizer. *Int. J. Photoenergy* **2012**, *2012*, 906198. [[CrossRef](#)]
39. Nunomura, S.; Minowa, A.; Sai, H.; Kondo, M. Mie scattering enhanced near-infrared light response of thin-film silicon solar cells. *Appl. Phys. Lett.* **2010**, *97*, 063507. [[CrossRef](#)]
40. Fielding, L.A.; Mykhaylyk, O.O.; Schmid, A.; Pontoni, D.; Armes, S.P.; Fowler, P.W. Visible Mie Scattering from Hollow Silica Particles with Particulate Shells. *Chem. Mater.* **2014**, *26*, 1270–1277. [[CrossRef](#)]
41. Koo, H.J.; Park, J.; Yoo, B.; Yoo, K.; Kim, K.; Park, N.G. Size-dependent scattering efficiency in dye-sensitized solar cell. *Inorg. Chim. Acta* **2008**, *361*, 677–683. [[CrossRef](#)]
42. Lu, H.; Huang, M.; Shen, K.S.; Zhang, J.; Xia, S.Q.; Dong, C.; Xiong, Z.G.; Zhu, T.; Wu, D.P.; Zhang, B.; et al. Enhanced Diffuse Reflectance and Microstructure Properties of Hybrid Titanium Dioxide Nanocomposite Coating. *Nanoscale Res. Lett.* **2018**, *13*, 328. [[CrossRef](#)]
43. Sanchezgil, J.A.; Nietovesperinas, M. Light-Scattering from Random Rough Dielectric Surfaces. *J. Opt. Soc. Am. A-Opt. Image Sci. Vis.* **1991**, *8*, 1270–1286. [[CrossRef](#)]
44. Maradudin, A.A.; Mendez, E.R. Light scattering from randomly rough surfaces. *Sci. Prog.* **2007**, *90*, 161–221. [[CrossRef](#)] [[PubMed](#)]
45. Wiersma, D.S. Disordered photonics. *Nat. Photonics* **2013**, *7*, 188–196. [[CrossRef](#)]
46. van de Lagemaat, J.; Frank, A.J. Effect of the surface-state distribution on electron transport in dye-sensitized TiO<sub>2</sub> solar cells: Nonlinear electron-transport kinetics. *J. Phys. Chem. B* **2000**, *104*, 4292–4294. [[CrossRef](#)]
47. Bisquert, J. Theory of the impedance of electron diffusion and recombination in a thin layer. *J. Phys. Chem. B* **2002**, *106*, 325–333. [[CrossRef](#)]
48. Wang, Q.; Moser, J.E.; Gratzel, M. Electrochemical impedance spectroscopic analysis of dye-sensitized solar cells. *J. Phys. Chem. B* **2005**, *109*, 14945–14953. [[CrossRef](#)]
49. Fabregat-Santiago, F.; Bisquert, J.; Palomares, E.; Otero, L.; Kuang, D.B.; Zakeeruddin, S.M.; Gratzel, M. Correlation between photovoltaic performance and impedance spectroscopy of dye-sensitized solar cells based on ionic liquids. *J. Phys. Chem. C* **2007**, *111*, 6550–6560. [[CrossRef](#)]
50. Andrade, L.; Sousa, J.; Ribeiro, H.A.; Mendes, A. Phenomenological modeling of dye-sensitized solar cells under transient conditions. *Sol. Energy* **2011**, *85*, 781–793. [[CrossRef](#)]
51. Sarker, S.; Ahammad, A.J.S.; Seo, H.W.; Kim, D.M. Electrochemical Impedance Spectra of Dye-Sensitized Solar Cells: Fundamentals and Spreadsheet Calculation. *Int. J. Photoenergy* **2014**, *2014*, 851705. [[CrossRef](#)]
52. Zdyb, A.; Krawczak, E. Organic Dyes in Dye-Sensitized Solar Cells Featuring Back Reflector. *Energies* **2021**, *14*, 5529. [[CrossRef](#)]

**Disclaimer/Publisher's Note:** The statements, opinions and data contained in all publications are solely those of the individual author(s) and contributor(s) and not of MDPI and/or the editor(s). MDPI and/or the editor(s) disclaim responsibility for any injury to people or property resulting from any ideas, methods, instructions or products referred to in the content.